HHS Public Access

Author manuscript

Nat Mater. Author manuscript; available in PMC 2017 May 07.

Published in final edited form as:

Nat Mater. 2017 March ; 16(3): 370–378. doi:10.1038/nmat4789.

Collagen intrafibrillar mineralisation as a result of the balance between osmotic equilibrium and electroneutrality

Li-na Niu[1,*], **Sang Eun Jee**[2,*], **Kai Jiao**[1], **Lige Tonggu**[3], **Mo Li**[3], **Liguo Wang**[3], **Yao-dong Yang**[4], **Ji-hong Bian**[4], **Lorenzo Breschi**[5], **Seung Soon Jang**[2], **Ji-hua Chen**[1], **David H. Pashley**[6], and **Franklin R. Tay**[6]

[1]State Key Laboratory of Military Stomatology & National Clinical Research Center for Oral Diseases & Shaanxi Key Laboratory of Oral Diseases, Department of Prosthodontics, School of Stomatology, The Fourth Military Medical University, Xi'an, China

[2]School of Materials Science and Engineering, Georgia Institute of Technology, Atlanta, Georgia, USA

[3]Department of Biological Structure, University of Washington, Seattle, Washington, USA

[4]Frontier Institute of Science and Technology, State Key Laboratory for Mechanical behavior of Materials, Xi'an Jiaotong University, Xi'an, China

[5]Department of Biomedical and Neuromotor Sciences, DIBINEM, University of Bologna, Bologna, Italy

[6]The Dental College of Georgia, Augusta University, Augusta, Georgia, USA

Abstract

Mineralisation of fibrillar collagen with biomimetic process-directing agents has enabled scientists to gain insight into the potential mechanisms involved in intrafibrillar mineralisation. Here, by using polycation- and polyanion-directed intrafibrillar mineralisation, we challenge the popular paradigm that electrostatic attraction is solely responsible for polyelectrolyte-directed intrafibrillar mineralisation. Because there is no difference when a polycationic or a polyanionic electrolyte is used to direct collagen mineralisation, we argue that additional types of long-range non-

Co-corresponding authors: Franklin R. Tay, The Dental College of Georgia, Augusta University, Augusta, Georgia, 30912-1129, USA. TEL: (706) 7212031, ftay@augusta.edu; Ji-hua Chen, School of Stomatology, The Fourth Military Medical University, Xi'an, China, jhchen@fmmu.edu.cn; Seung Soon Jang, School of Materials Science and Engineering, Georgia Institute of Technology, Atlanta, Georgia, USA, seungsoon.jang@mse.gatech.edu.
Correspondence and requests for materials should be addressed to F.R.T. at ftay@augusta.edu.
*These authors contributed equally to this work

Supplementary Information is linked to the online version of the paper at www.nature.com/naturematerials.

Author contributions

L.N. and K.J. performed the mineralisation experiments and analytical part of the study and wrote the manuscript. S.E.J. and S.S.J. contributed to the molecular dynamic simulation. L.T., M.L. and L.W. performed cryo-TEM examination. J.B. and Y.Y. contributed to the atomic force microscopy. J.C., L.B. and D.H.P. provided advice on the experimental design and edited the manuscript. F.R.T. performed ultramicrotomy, TEM examination, supervised the project and wrote the manuscript. All authors discussed the results and revised the manuscript.

The authors declare no competing financial interests.

electrostatic interactions are responsible for intrafibrillar mineralisation. Molecular dynamics simulations of collagen structures in the presence of extrafibrillar polyelectrolytes show that the outward movement of ions and intrafibrillar water through the collagen surface occurs irrespective of the charges of polyelectrolytes, resulting in the experimentally verifiable contraction of the collagen structures. The need to balance electroneutrality and osmotic equilibrium simultaneously to establish Gibbs-Donnan equilibrium in a polyelectrolyte-directed mineralisation system establishes a new model for collagen intrafibrillar mineralisation that supplements existing collagen mineralisation mechanisms.

Extensive work on collagen mineralisation during their self-assembly[1], as well as the use of process-directing agents for mineralisation of fibrillar collagen[2–5], have enabled scientists to gain seminal insight into the potential mechanisms involved in intrafibrillar mineralisation[6–10]. Among these efforts, the discovery of prenucleation clusters and the polymer-induced liquid precursor concept have revolutionised current thinking on how intrafibrillar mineralisation may be achieved[4,6,10,11]. Phenomenological observation of "a-band docking" of polyanion-stabilised mineralisation precursors on positively-charged regions of a collagen fibril[4,12] has also been instrumental in advancing the concept of Columbic attraction[13,14] as the prevailing mechanism for intrafibrillar mineralisation. Although polycations such as poly(allylamine) hydrochloride (PAH) also induce liquid-liquid phase separation and stabilisation of crystallisation precursors[15,16], polycation-directed intrafibrillar mineralisation of collagen with calcium phosphate mineral phases has not been examined before now because of the operating assumption that there would be electrostatic repulsion. Here, PAH-directed intrafibrillar mineralisation is used to set the stage for challenging the paradigm that electrostatic attraction is responsible for polyelectrolyte-directed intrafibrillar collagen mineralisation. Using additional cationic and anionic collagen models for polycation- and polyanion-stabilised mineralisation precursors respectively, electrostatic interactions are inadequate in accounting for intrafibrillar uptake of those calcium phosphate precursors. By determining the selective permeability of fibrillar collagen to molecules of different sizes, additional colligative interactions are predicted to be involved through the establishment of Gibbs-Donnan equilibrium[17] between the extrafibrillar and intrafibrillar milieu. Molecular dynamics simulations of collagen structures in the presence of extrafibrillar polyelectrolytes show that outward movement of monovalent ions and intrafibrillar water through the collagen surface occurs irrespective of the charges of the polyelectrolytes, and results in experimentally verifiable contraction of the collagen structures at the fibrillar level. Inflation of the poroelastic[18], contracted collagen fibrils in water causes influx of hydrated mineralisation precursors into the intrafibrillar compartments. The need to balance electroneutrality and osmotic equilibrium simultaneously in a polyelectrolyte-directed mineralisation system establishes a new paradigm for collagen intrafibrillar mineralisation.

Characterisation of PAH-ACP

The minimal PAH concentration (200 μg/mL; Mw 15 kDa, pKa 8.7) that stabilised a supersaturated mineralisation solution (4.5 mM $CaCl_2{\cdot}2H_2O$ and 2.1 mM K_2HPO_4) for 5 days without turbid precipitations was characterised by dynamic light scattering and zeta

potential measurements. This solution, designated as PAH-stabilised amorphous calcium phosphate precursor phases (PAH-ACP), was used in subsequent experiments. The PAH-ACP has a mean hydrodynamic diameter of 17.9 nm (Supplementary Information (SI); Fig. SI-2a) and zeta potential of 21.48 mV (Fig. SI-2b). For comparison, calcium phosphate (CaP) complexes stabilised by poly(aspartic acid) (PAsp) have a mean hydrodynamic diameter of 18.6 nm (Fig. SI-2c) and zeta potential of −22.65 mV (Fig. SI-2d).

Cryogenic transmission electron microscopy (TEM) was used for examining non-turbid PAH-ACP-containing solutions prior to vitrification in melting ethane (Fig. SI-3). This was performed to ascertain that features subsequently identified using conventional TEM did not represent desiccation-associated structural alterations. Solutions examined within 15 min after preparation showed the smallest discernible CaP aggregation that appeared as electron-dense aggregates (Fig. SI-3, a–b). They corresponded to the early stage of prenucleation cluster formation in CaP mineralising solutions[6,19]. Images taken from vitrified solutions after 24 h showed evidence of ensemble densification (Fig. SI-3c). Continued densification resulted in branched polymeric assemblies (Fig. SI-3d) and irregular PAH-stabilised ACP (Fig. SI-3e) after 3 days. Figure SI-3f schematically illustrates the characteristics of the prenucleation clusters. Although the formation of a liquid precursor mineral phase has been reported by Gower *et al.* in the calcium carbonate system[20], experimental verification of a liquid precursor phase in the CaP system has not been established to-date[10]. It is possible that liquid CaP precursors with definitive phase boundaries are produced via liquid-liquid phase separation[21] from highly dynamic, phase boundary-free prenucleation clusters[19,22,23].

PAH-ACP induced intrafibrillar mineralisation

Cryogenic TEM (Fig. 1, a–d) was used for study of polycation-directed collagen mineralisation**,** using a single-layer mineralisation model comprising reconstituted type I collagen fibrils. A tilt series of a mineralised collagen fibril acquired by cryo-electron tomography (Fig. 1e; Movie S1-tilt.mov) was employed for 3-D reconstruction (Fig. 1, f–h; Movie S2-reconstruction.mov), to confirm the presence of intrafibrillar mineralisation. Because ultrastructural features of PAH-ACP seen in cryogenic TEM (Fig. SI-3) were identifiable in conventional TEM of collagen mineralisation (Fig. SI-4), the latter was employed for detailed examination of intrafibrillar mineralisation by PAH-ACP. Unstained fibrils were heavily mineralised after 48 h (Fig. 2a). Uranyl acetate-stained collagen fibrils mineralised for 48 h showed arrangement of apatite crystallites along the fibril's c-axis (Fig. 2b), as demonstrated by the 002 Debye arc obtained from selected area electron diffraction (SAED) of the intrafibrillar minerals. Intrafibrillar ACP was more readily seen in fibrils that were mineralised for less than 24 h (Fig. 2c). After infiltration with ACP, the overlap and gap zones had similar band intensities; after ACP was transformed into apatite, band intensities in the overlap zone were higher than those in the gap zone, and the a-band of the gap zone showed the lowest relative band intensity (Fig. 2d). Stained collagen mineralised for 12–18 h showed accumulation of PAH-stabilised CaP complexes on the collage surface with no predilection of band location (i.e. a–e bands) along which infiltration of these complexes occurred (Fig. 2, e–g). Filamentous structures similar to those identified by cryogenic TEM (Fig. SI-3b) were present in the vicinity of the collagen fibril (Fig. 2g). According to the paradigm of Coulomb attraction between polyanion-stabilised CaP

complexes and net positive charges present on the a-bands of collagen[4], intrafibrillar infiltration of PAH-ACP could not have occurred in the a-bands. Likewise, PAH-ACP should not have been attracted to the other band sites (e.g. b, c and d bands) because charges of the ionic residues in the fibrillar polyampholyte are internally compensated along those locations[24,25].

Cationic and anionic collagen mineralisation models

To test the hypothesis that short-ranged electrostatic interaction based on the Poisson-Boltzmann equation is the sole driving force responsible for intrafibrillar infiltration of mineralisation precursors, additional positive charges were introduced on collagen, which should result in reduction/absence of intrafibrillar mineralisation, whereas the opposite should occur when additional negative charges were introduced. These cationic (Fig. 3) and anionic collagen models (Fig. SI-5) were used as mineralisation templates for PAH-directed collagen mineralisation. For cationic collagen, polycations (PAH) were conjugated to collagen fibrils (original zeta potential: 2.5±0.13 mV) via amino acids containing carboxyl side chains (Fig. 3a), resulting in collagen sponges with positive surface zeta potential (18.56±1.02 mV; Fig. 3b), increased amine groups and decreased carboxyl groups (Fig. 3c), and post-modification change identifiable by attenuated total reflection-Fourier transform infrared spectroscopy (ATR-FTIR; Fig. SI-6a). Surprisingly, conventional TEM revealed excellent mineralisation results that were contrary to our expectations. Intrafibrillar mineralisation was much more rapid; extensive mineralisation was observed in 3-D collagen sponges as early as in 1 day (Fig. 3d) compared with unmodified sponges (Fig. SI-7). Heavily-mineralised collagen with banding patterns was observed after 7 days (Fig. 3e), similar to mineralisation of unmodified sponges (Fig. SI-7). Similar results were observed in the mineralisation of single-layer collagen fibrils (Fig. SI-8). Analogous conflicting results were observed in the anionic collagen model (Figs. SI-5, SI-6b, SI-8) in which polyanions (PAsp) were conjugated to collagen via amino acids containing amine side chains. Intrafibrillar mineralisation was slow and sparse, with coacervates of large ACP adsorbed on the collagen surface and profuse extrafibrillar mineralisation. Similar results were identified in the cationic and anionic collagen models mineralized with PAsp-ACP (Fig. SI-9). Thus, the hypothesis that short-ranged electrostatic interaction is the sole driving force responsible for intrafibrillar infiltration of PAH-ACP has to be rejected. Rejection of the aforementioned hypothesis does not mean that electrostatic attraction does not play a role in collagen mineralisation; it suggests that attraction of polyelectrolyte-stabilised prenucleation clusters or ACP toward the collagen fibrils may be controlled by additional driving forces that have not been previously reported in the literature.

Whereas electrostatic interaction was proposed as the driving force for attracting prenucleation clusters to the collagen fibril surface, capillary infiltration, has been proposed by Gower as a potential transportation mechanism for migration of mineralisation precursors into the internal water compartments of the collagen fibril. In capillary infiltration, polymer-stabilised liquid precursors are “drawn into the collagen interstices by capillary forces generated at the interface between two immiscible liquids”[10,20,26]. Although this hypothesis is attractive, it relies on the existence of mineralisation precursors in a liquid state, which we were unable to verify experimentally in the present work. Hence, capillary infiltration of

PAH-ACP into collagen was not further investigated and the existence of liquid-within-liquid capillary action remains an open question.

Selective permeability of collagen

Molecules larger than 40 kDa are excluded from the intrafibrillar water compartments of fibrillar collagen, whereas molecules smaller than 6 kDa can freely access all the intrafibrillar water[27]. These phenomena formed the basis of "mineralisation by inhibitor exclusion" hypothesis, wherein globular protein nucleation inhibitors such as fetuin that are too large to enter the intrafibrillar milieu indirectly promote intrafibrillar nucleation of the infiltrated mineral[28]. To examine if this hypothesis is applicable to PAH-directed intrafibrillar mineralisation, and how the process is affected by oligoelectrolytes that can freely access all the intrafibrillar water, size exclusion chromatography with demineralised bone powder collagen as the stationary phase[27,29] was used to study the elution profiles of a pair of amine-containing molecules (PAH, Mw 15 kDa *vs* spermine, 202 Da) and a pair of carboxylic acid-containing molecules (PAsp, 27 kDa *vs* citric acid, 192 Da), using dimethyl sulphoxide (78 Da) and bovine serum albumin (66 kDa) as the respective low and high molecular weight controls. Elution profiles of PAH, spermine and PAH/spermine mixture are shown in Fig. 4a, those of the negative and positive controls in Fig. SI-10a, and those of PAsp, citric acid and PAsp/citric acid mixture are shown in Fig. SI-10b. Elution volumes derived from these data were used with the calculated intrafibrillar volume of the demineralised bone collagen to yield the vol% of intrafibrillar water exposed to test molecules (Table SI-10). Whereas small charged molecules such as spermine (98.64%) and citric acid (99.34%) could almost completely access collagen intrafibrillar water, PAH and PAsp could only access 50.5% and 32.67% of the intrafibrillar water, respectively (Fig. 4b). Although PAH and PAsp were not completely size-excluded from the intrafibrillar milieu, these polyelectrolyte nucleation inhibitors were capable of producing excellent intrafibrillar mineralisation (Fig. 2a, Fig. SI-10e). When spermine was added to PAH-containing mineralising solution, the rate of intrafibrillar mineralisation was substantially reduced[30], although apatite nucleation still occurred within the fibrils (Fig. 4c). Similar results were achieved when citric acid was incorporated in PAsp-containing mineralising solution (Fig. SI-10d)[31]. The size exclusion data clearly established that collagen fibrils possess the properties of a selectively-permeable membrane, and that long-ranged interactions may be involved during intrafibrillar mineralisation of collagen. The findings that PAH or PAsp can partially access collagen intrafibrillar water do not mean that collagen fibrils are not selectively-permeable; their selective-permeability is non-ideal, with osmotic reflection coefficients that are smaller than unity[32].

Establishment of Gibbs-Donnan equilibrium

When two aqueous compartments with different solute concentrations are separated by a selectively-permeable membrane, water moves down its concentration gradient from the low osmolarity to the high osmolarity compartment. For salt-free solutions of polyelectrolytes, the osmotic pressure exceeds that of neutral polymers at similar polymer concentrations by several orders of magnitude[33]. Although cationic or anionic polyelectrolytes are engaged in stabilising CaP aggregates, the solutions still exhibit high positive or negative zeta potentials

(Fig. SI-2). The effect of cationic or anionic polyelectrolyte concentration on the osmolality of polyelectrolyte-stabilised ACP was determined (Fig. SI-11A). For PAH concentration of 200 μg/mL, the osmolality of PAH-ACP was 335 mOsm/Kg, while that of PAH in water was 17 mOsm/Kg (a 20-fold difference). The data indicates that free PAH (i.e. not involved in stabilisation of CaP aggregates) is unlikely to exert much oncotic pressure in the presence of a selectively-permeable membrane, as predicted by Manning-Oosawa counterion condensation on the polyelectrolyte that reduces its net surface charge density[34]. In the presence of a salt, osmotic pressure of the PAH-ACP solution is predominantly derived from osmotically-active counterions (i.e. those not involved in counterion condensation) and salt ions (Na^+, Cl^-) present in the mineralising solution[33]. Establishment of Gibbs-Donnan equilibrium[35] between the intrafibrillar and extrafibrillar water compartments of collagen represents a means of providing the long-ranged interactions for ACP to infiltrate into fibrillar collagen (Fig. SI-11B). Gibbs-Donnan equilibrium involves establishing both electroneutrality and osmotic equilibrium across a selectively-permeable membrane. Positively-charged electrolytes completely or partially impermeable to the intrafibrillar fluid compartments of collagen attract negatively-charged ions and repel positively-charged ions. The passive distribution of cations is thus altered to preserve electroneutrality in the extrafibrillar and intrafibrillar compartments. The diffusible cation concentration is lower in the extrafibrillar compartment containing PAH-ACP with positive zeta potential. Thus, cations such as Na^+ will move out of the intrafibrillar compartment into the extrafibrillar compartment. The excess positive charges render the extrafibrillar compartment positive in terms of electrochemical potential. To establish electrochemical equilibrium across the selectively-permeable membrane, anions such as Cl^- have to move out of the intrafibrillar compartment. The consequence of establishing Gibbs-Donnan equilibrium is that there are more osmotically-active species in the extrafibrillar than the intrafibrillar compartment at equilibrium. The total osmolar concentration is higher in the extrafibrillar compartment; the extra osmotic force from diffusible salt ions and uncondensed counterions results in water moving out of the intrafibrillar compartment to establish osmotic equilibrium. The net result of the Gibbs-Donnan effect is that more water moves into the extrafibrillar compartment than would be predicted on the basis of oncotic pressure of the PAH molecules alone. Partitioning of osmotically-active counterions and salt ions across membrane impermeable to polyelectrolyte chains to establish Gibbs-Donnan equilibrium[36] has been exhaustively modelled using Monte Carlo simulations[37].

Molecular dynamics simulation

To validate the existence of Gibbs-Donnan equilibrium and to examine how this affects the dimension of collagen fibrils, full atomistic molecular dynamics simulation of a high-resolution hydrated collagen structure was used to investigate the transport of ions and water molecules from the intrafibrillar to the extrafibrillar region of collagen fibrils in the presence of polyanionic and polycationic process-directing agents, respectively (Fig. 5a; numerical data in SI-12). The structure of equilibrated collagen was verified by analysing the three hydration layers (Fig. 5b; corresponding to tightly-bound, loosely-bound and free water molecules) and charge density along the c-axis (Fig. 5c). The a- and c-band regions exhibit positive charge densities as previously reported[4]. Collagen structures with water molecules

in the intrafibrillar and extrafibrillar regions are depicted in Fig. 5d. The number of Na ions (Fig. 5e) and Cl ions (Fig. 5f) in the intrafibrillar region decreased as simulation time increases in both systems, irrespective of the charges of the polyelectrolyte. This indicates diffusion of both ions from the intrafibrillar region to the extrafibrillar region. The water molecules in intrafibrillar regions also decreased in both systems (Fig. 5g), following the migration of Na and Cl ions into the extrafibrillar region of the collagen fibrils. Most of the water molecules were removed from the gap regions, where there are more loosely-bound and free water molecules filling the intrafibrillar spaces (Fig. 5a). Thus, in the presence of strong polyelectrolytes near the collagen surface, most of the water molecules diffuse out of the gap regions.

To examine the effect of migration of monovalent ions and intrafibrillar water on dimensional changes in collagen structures, Root Mean Square Deviations (RMSD) of collagen molecules was analysed between atomic position at time t and the initial positions of backbone atoms. The RMSD of collagen backbones exhibited steep increases (Fig. 5h), indicating contraction of the collagen molecules. Solvent Accessible Surface Area (SASA) of the collagen structures decreased over simulation time in both polyanionic and polycationic systems (Fig. 5i), inferring contractions of the collagen structures. SASA was calculated based on the double cubic lattice method[38]. After the ions and water molecules diffused out of the intrafibrillar water compartments into the extrafibrillar region (Fig. 5e–g), SASA of collagen molecules decreased from 3844.64 nm^2 to 3799.86 nm^2 (1.16% decrease) in the polyanionic system, and from 3783.54 nm^2 to 3746.11 nm^2 (0.99% decrease) in the polycationic system over a period of 20 ns. Combined with the observation that water molecules mainly diffuse from the gap region, it may be inferred that SASA mainly decreases in the gap regions where more spaces are initially filled by water molecules (SI-12).

Dimensional changes derived from simulated collagen structures were also experimentally verified by examination of collagen reconstituted on freshly-cleaved mica using atomic force microscopy (SI-13). Addition of PAH or PAsp to NaCl-containing HEPES buffer resulted in statistically significant reduction in the diameter of the fibrils. When the incubation medium was changed to HEPES buffer containing 200 μg/mL PAH (or 75 μg/mL PAsp), 4.5 mM $CaCl_2{\cdot}2H_2O$ and 2.1 mM K_2HPO_4, the diameter of the contracted fibrils increased significantly. Because of the inherent viscoelasticity of collagen fibrils[39,40], we hypothesise that the contracted fibrils would inflate to restore the intrafibrillar volume[41,42] in a manner analogous to the expansion of a compressed sponge immersed in water[43]. This stress relaxation provides the driving mechanism[44] for the influx of the polyelectrolyte-stabilised mineralisation precursors. Molecular dynamics simulation was performed to test this hypothesis (Fig. 6, SI-14). Upon the introduction of CaP precursors (simplified as Ca ions) into the system, the quantity of Ca ions in the intrafibrillar regions increased over time in both systems (Fig. 6d). During CaP infiltration, SASA of the contracted collagen structure, which was 3746.11 nm^2 without Ca ions, increased to 3762.21 nm^2 (0.43% increase) in the polycationic system while SASA increased from 3799.86 nm^2 to 3874.33nm^2 (1.96 % increase) in the polyanionic system. The results infer that re-swelling of the contracted collagen causes infiltration of CaP precursors into the intrafibrillar regions (Fig. 6e,f). While stress-induced intrafibrillar diffusion of Ca ions was observed in both systems, significantly

larger swelling was observed in polyanionic system than in polycationic system. Compared to SASA of initial collagen structures before polyelectrolyte-induced contraction, the collagen inflated to 100.77 % of the initial surface area (3844.64 nm^2) in the polyanionic system, while collagen structure in the polycationic system recovered 99.44% of its initial surface area (3783.53 nm^2). This structural difference would be caused by the stronger electrostatic attractions between positively-charged collagen and negatively-charged polyelectrolytes in the polyanionic system. Due to inflation of the collagen structures, intrafibrillar water increased in polyanionic system while it decreased in polycationic system (Fig. 6c) and the decrease of Na and Cl ions in intrafibrillar region was more evident in the polycationic system (Fig. 6a–b). We opine that both polycationic and polyanionic electrolytes cause structural contraction and re-swelling to direct collagen mineralisation in long-range interaction. Nevertheless, short-range electrostatic attraction enhances this stress-induced infiltration.

Outlook

The observation that both polycationic and polyanionic process-directing agents may be used for mineralisation of pre-assembled fibrillary collagen highlights the need to maintain osmotic equilibrium and electroneutrality in a polyelectrolyte-directed mineralisation system. Hence, we construed that long-range interactions are involved through establishment of Gibbs-Donnan equilibrium, which, together with short-range electrostastic interactions, provide the driving forces for infiltration of polyelectrolyte-stabilised prenucleation clusters into the water compartments of collagen to initiate intrafibrillar mineralisation.

Methods

Full details of the mineralisation strategy and sample characterisation techniques used are presented in the Supplementary Information.

Supplementary Material

Refer to Web version on PubMed Central for supplementary material.

Acknowledgments

This work was supported by grant 2015AA020942 from National High Technology Research and Development Program of China, grant R01 DE015306-06 from NIDCR, grant 81400555, 81130078, 81671012 and 81530050 from NSFC, program IRT13051 from Changjiang Scholars and Innovative Research Team in University and Innovative Research Team in University and Young Elite Scientist Sponsorship Program by CAST. We thank L. B. Gower (University of Florida, Florida, USA) for discussion of some of the results.

References

1. Wang Y, et al. The predominant role of collagen in the nucleation, growth, structure and orientation of bone apatite. Nat Mater. 2012; 11:724–733. [PubMed: 22751179]
2. Olszta MJ, et al. Bone structure and formation: A new perspective. Mater Sci & Eng. 2007; 58:77–116.
3. Deshpande AS, Beniash E. Bio-inspired synthesis of mineralized collagen fibrils. Cryst Growth Des. 2008; 8:3084–3090.

4. Nudelman F, et al. The role of collagen in bone apatite formation in the presence of hydroxyapatite nucleation inhibitors. Nat Mater. 2010; 9:1004–1009. [PubMed: 20972429]
5. Liu Y, et al. Hierarchical and non-hierarchical mineralisation of collagen. Biomaterials 2011. 2011; 32:1291–1300.
6. Habraken WJ, et al. Ion-association complexes unite classical and non-classical theories for the biomimetic nucleation of calcium phosphate. Nat Commun. 2013; 4:1507. [PubMed: 23422675]
7. Nudelman F, Lausch AJ, Sommerdijk NA, Sone ED. In vitro models of collagen biomineralization. J Struct Biol. 2013; 183:258–269. [PubMed: 23597833]
8. Wang Y, et al. Water mediated structuring of bone apatite. Nat Mater. 2013; 12:1144–1153. [PubMed: 24193662]
9. Xu Z, et al. Molecular mechanisms for intrafibrillar collagen mineralization in skeletal tissues. Biomaterials. 2015; 39:59–66. [PubMed: 25477172]
10. Gower, LB. Biomimetic mineralization of collagen. In: Aparicio, C., Ginebra, MP., editors. Biomineralization and Biomaterials: Fundamentals and Applications. 1. Vol. Ch 6. Woodhead Publishing, Elsevier Ltd; Cambridge, United Kingdom: 2016.
11. Jee SS, Thula TT, Gower LB. Development of bone-like composites via the polymer-induced liquid-precursor (PILP) process. Part 1: influence of polymer molecular weight. Acta Biomater. 2010; 6:3676–3686. [PubMed: 20359554]
12. Cölfen H. Biomineralization: A crystal-clear view. Nat Mater. 2010; 9:960–961. [PubMed: 21102512]
13. Li ST, Katz EP. An electrostatic model for collagen fibrils. The interaction of reconstituted collagen with Ca++, Na+, and Cl−. Biopolymers. 1976; 15:1439–1460. [PubMed: 963243]
14. Silver FH, Landis WJ. Deposition of apatite in mineralizing vertebrate extracellular matrices: A model of possible nucleation sites on type I collagen. Connect Tissue Res. 2011; 52:242–254. [PubMed: 21405976]
15. Xu AW, Antonietti M, Cölfen H, Fang YP. Uniform hexagonal plates of vaterite $CaCO_3$ mesocrystals formed by biomimetic mineralization. Adv Funct Mater. 2006; 16:903–908.
16. Cantaert B, et al. Think positive: phase separation enables a positively charged additive to induce dramatic changes in calcium carbonate morphology. Adv Func Mater. 2012; 22:907–915.
17. Philipse A, Vrij A. The Donnan equilibrium: I. On the thermodynamic foundation of the Donnan equation of state. J Phys Condens Matter. 2011; 23:194106. [PubMed: 21525564]
18. Chandran PL, Barocas VH. Microstructural mechanics of collagen gels in confined compression: poroelasticity, viscoelasticity, and collapse. J Biomech Eng. 2004; 126:152–166. [PubMed: 15179845]
19. Dey A, et al. The role of prenucleation clusters in surface-induced calcium phosphate crystallization. Nat Mater. 2010; 9:1010–1014. [PubMed: 21076415]
20. Gower LB, Odom DJ. Deposition of calcium carbonate films by a polymer-induced liquid-precursor (PILP) process. J Cryst Growth. 2000; 210:719–734.
21. Hyman AA, Weber CA, Jülicher F. Liquid-liquid phase separation in biology. Annu Rev Cell Dev Biol. 2014; 30:39–58. [PubMed: 25288112]
22. Bewernitz MA, Gebauer D, Long J, Cölfen H, Gower LB. A metastable liquid precursor phase of calcium carbonate and its interactions with polyaspartate. Faraday Discuss. 2012; 159:291–312.
23. Gebauer D, Kellermeier M, Gale JD, Bergström L, Cölfen H. Pre-nucleation clusters as solute precursors in crystallisation. Chem Soc Rev. 2014; 43:2348–2371. [PubMed: 24457316]
24. Weinstock A, King PC, Wuthier RE. The ion-binding characteristics of reconstituted collagen. Biochem J. 1967; 102:983–988. [PubMed: 16742518]
25. Li S, Golub E, Katz EP. Electrostatic side chain complementarity in collagen fibrils. J Mol Biol. 1975; 98:835–839. [PubMed: 513]
26. Gower LB. Biomimetic model systems for investigating the amorphous precursor pathway and its role in biomineralization. Chem Rev. 2008; 108:4551–4627. [PubMed: 19006398]
27. Toroian D, Lim JE, Price PA. The size exclusion characteristics of type I collagen: implications for the role of noncollagenous bone constituents in mineralization. J Biol Chem. 2007; 282:22437–22447. [PubMed: 17562713]

28. Price PA, Toroian D, Lim JE. Mineralization by inhibitor exclusion: the calcification of collagen with fetuin. J Biol Chem. 2009; 284:17092–17101. [PubMed: 19414589]
29. Takahashi M, et al. The importance of size-exclusion characteristics of type I collagen in bonding to dentin matrices. Acta Biomater. 2013; 9:9522–9528. [PubMed: 23928333]
30. Mueller E, Sikes CS. Adsorption and modification of calcium salt crystal growth by anionic peptides and spermine. Calcif Tissue Int. 1993; 52:34–41. [PubMed: 8384046]
31. Rhee S-H, Tanaka J. Effect of citric acid on the nucleation of hydroxyapatite in a simulated body fluid. Biomaterials. 1999; 20:2155–2160. [PubMed: 10555083]
32. Bhalla G, Deen WM. Effects of charge on osmotic reflection coefficients of macromolecules in porous membranes. J Colloid Interface Sci. 2009; 333:363–372. [PubMed: 19211110]
33. Dobrynin AV, Rubinstein M. Theory of polyelectrolytes in solutions and at surfaces. Prog Polym Sci. 2005; 30:1049–1118.
34. O'Shaughnessy B, Yang Q. Manning-Oosawa counterion condensation. Phys Rev Lett. 2005; 94:048302. [PubMed: 15783607]
35. Nguyen MK, Kurtz I. Quantitative interrelationship between Gibbs-Donnan equilibrium, osmolality of body fluid compartments, and plasma water sodium concentration. J Appl Physiol (1985). 2006; 100:1293–1300. [PubMed: 16357067]
36. Alexandrowicz Z, Katchalsky A. Colligative properties of polyelectrolyte solutions in excess of salt. J Polym Sci Part A. 1963; 1:3231–3260.
37. Carrillo J-MY, Dobrynin AV. Salt effect on osmotic pressure of polyelectrolyte solutions: simulation study. Polymers. 2014; 6:1897–1913.
38. Eisenhaber F, Lijnzaad P, Argos P, Sander C, Scharf M. The double cubic lattice method: Efficient approaches to numerical integration of surface area and volume and to dot surface contouring of molecular assemblies. J Comput Chem. 1995; 16:273–284.
39. Shen ZL, Kahn H, Ballarini R, Eppell SJ. Viscoelastic properties of isolated collagen fibrils. Biophys J. 2011; 100:3008–3015. [PubMed: 21689535]
40. Sopakayang R, De Vita R, Kwansa A, Freeman JW. Elastic and viscoelastic properties of a type I collagen fiber. J Theor Biol. 2012; 293:197–205. [PubMed: 22037061]
41. Masic A, et al. Osmotic pressure induced tensile forces in tendon collagen. Nat Commun. 2015; 6:5942. [PubMed: 25608644]
42. Kwansa AL, Freeman JW. Elastic energy storage in an unmineralized collagen type I molecular model with explicit solvation and water infiltration. J Theor Biol. 2010; 262:691–697. [PubMed: 19878687]
43. Sachs F, Sivaselvan MV. Cell volume control in three dimensions: Water movement without solute movement. J Gen Physiol. 2015; 145:373–380. [PubMed: 25870207]
44. Screen HRC, Seto J, Krauss S, BoeSecke P, Gupta HS. Extrafibrillar diffusion and intrafibrillar swelling at the nanoscale are associated with stress relaxation in the soft collagenous matrix tissue of tendons. Soft Matter. 2011; 7:11243–11251.

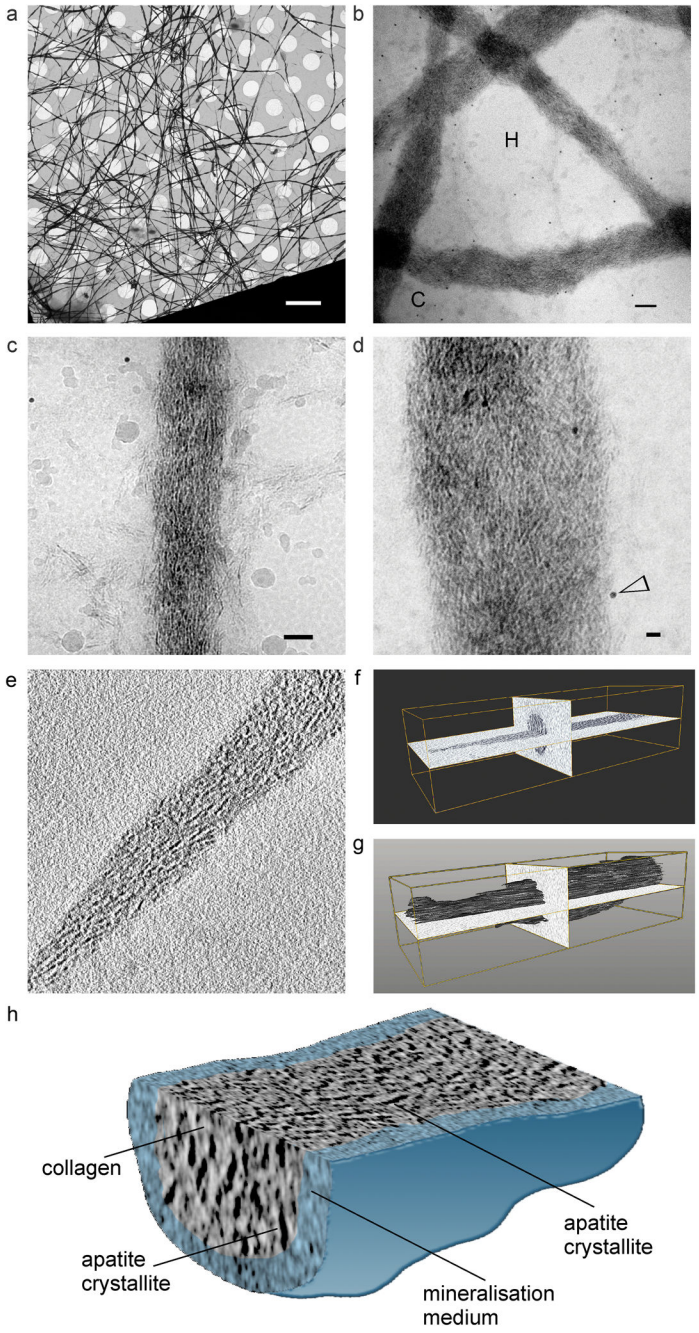

Figure 1.

Cryogenic TEM images of **a**) vitrified collagen fibrils mineralised by PAH-ACP (bar: 5 μm). **b**) Higher magnification image of several mineralised collagen fibrils (bar: 100 nm). C: carbon film; H: holes within carbon film. **c**) Higher magnification of a single mineralised collagen fibril (bar: 50 nm). Minor ice contamination can be seen. **d**) High magnification of intrafibrillar mineral deposits within mineralised collagen fibrils (probably overlapping of two fibrils) (bar: 20 nm). Electron-dense spots (open arrowhead) represent 10 nm gold particles added as fiducial markers for image alignment in electron tomography. 3-D

reconstruction from a cryo-electron tomography tilt series (unstained, movie available as Movie S1-tilt.mov) of a collagen fibril mineralised by polycation (PAH)-directed intrafibrillar mineralisation. **e**) A “half z-plane” image reconstructed by IMOD 4.7. **f**) and **g**) Segmentation of the 3-D volume confirmed that intrafibrillar mineralisation occurred within the collagen fibril (movie available as Movie S2-reconstruct.mov). **h**) Visualisation of 3-D volume of one part of the mineralised fibril. The mineralisation medium was artificially-coloured. Image shows orientation of apatite crystallites within the mineralised collagen fibril.

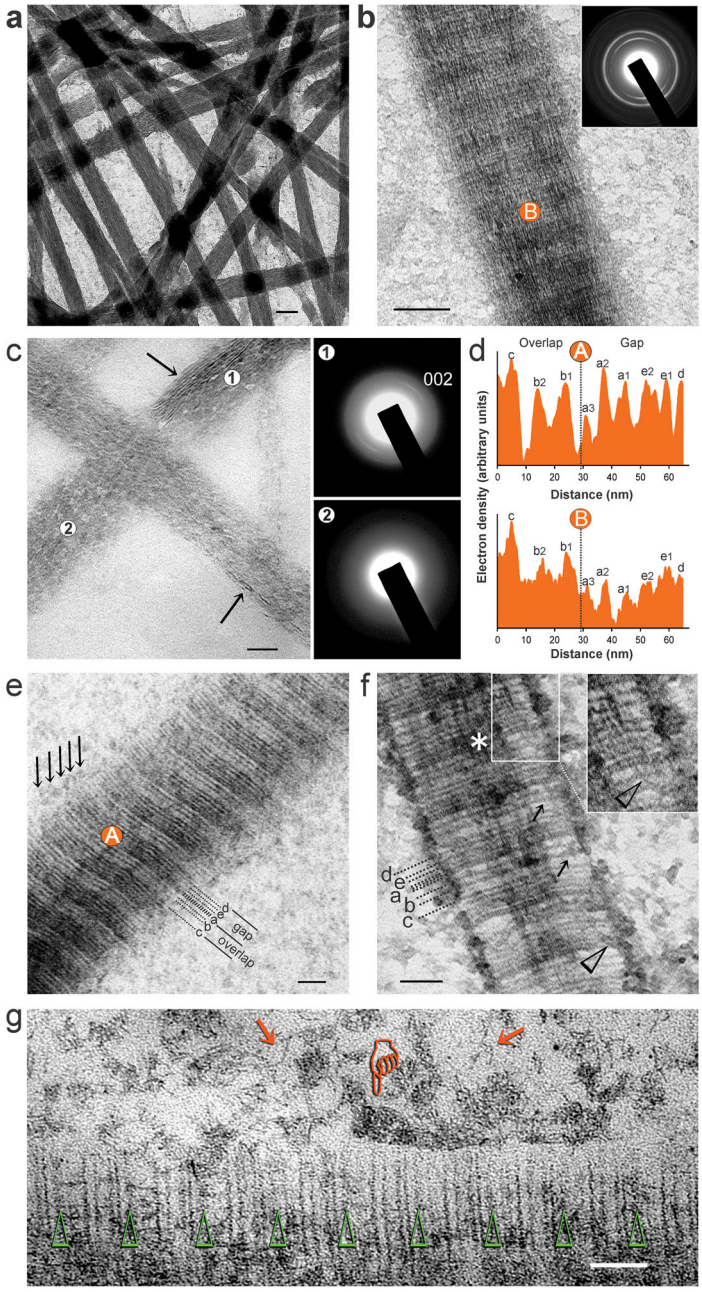

Figure 2.

Conventional TEM of mineralisation of reconstituted collagen fibrils by PAH-ACP (single-layer collagen mineralisation model). **a**) Unstained fibrils were heavily mineralised after 48 h (bar: 100 nm). **b**) Uranyl acetate-stained collagen mineralised for 48 h (bar: 200 nm). Selected area electron diffraction (SAED; inset) shows apatite crystallites aligned along the fibril's c-axis. **c**) Unstained collagen mineralised for 24 h (bar: 50 nm). Fibrils were predominantly filled with ACP (SAED, location 2). Apatite crystallites (SAED, location 1) could be identified within a diffuse bed of ACP in some locations (arrows). **d**) Band intensity profiles from a representative D-spacing obtained from ACP-filled, stained

collagen (location A in "**e**"), and apatite-filled, stained collagen (location B in "**b**"). Dashed lines delineate border between overlap and gap zones. **e**) Stained ACP-filled collagen mineralised for 12 h with ACP still infiltrating into the fibril (bar: 25 nm). There was no predilection of band location (i.e. a–e bands) along which ACP infiltration occurred (arrows). **f**) Stained collagen mineralised for 12 h (bar: 50 nm). CaP complexes could be identified in the fibril's periphery (arrows). Inset: communication of CaP complexes from the fibril's surface with ACP in the intrafibrillar spaces (arrowheads) supports the fluidic nature of mineralisation precursors. **g**) Stained collagen mineralised for 18 h with commencement of intrafibrillar apatite crystallisation (bar: 50 nm). Arrowheads: a-band positions. There is no particular band location that preferentially attracted the attachment of branched PAH-stabilised CaP complexes and ACP aggregates (pointer). Filamentous structures similar to those observed by cryogenic TEM can be identified close to the fibril's surface (arrows).

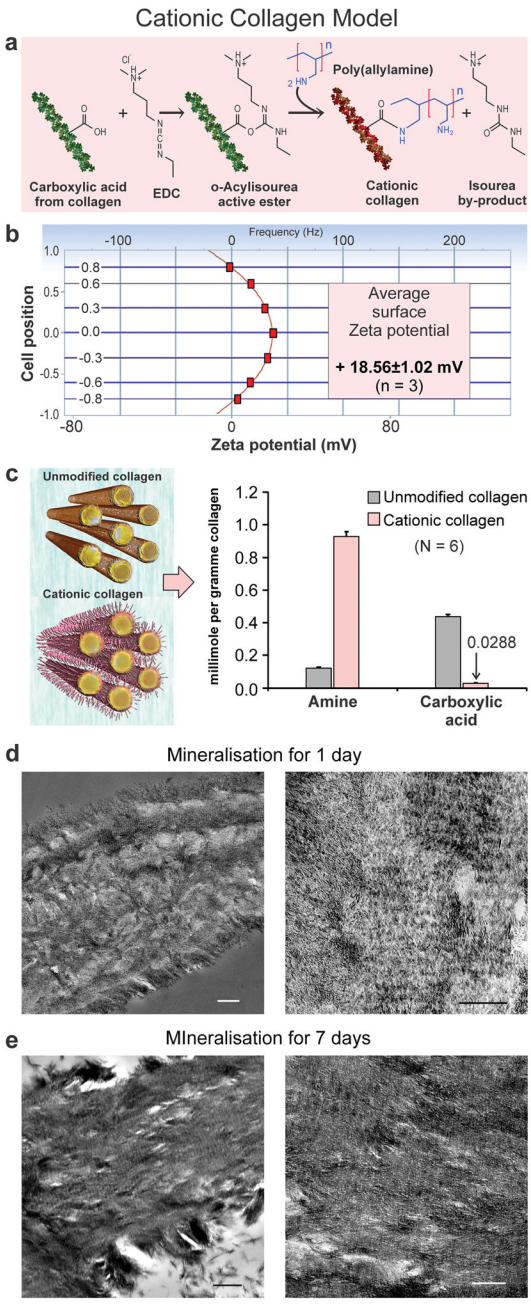

Figure 3.

Cationic collagen model of PAH-ACP intrafibrillar mineralisation. **a**) Method of conjugation of polycations (PAH) to collagen fibrils via amino acids containing –COOH side chains. EDC: carbodiimide. **b**) Surface zeta potential of cationic collagen was determined from the measured positive electrophoretic mobility of probe particles. **c**) Comparison of free amine and carboxyl groups between cationic and unmodified collagen. Decrease in carboxyl groups is due to their conjugation with PAH via the O=C−N-H linkage. **d**) TEM of leaflets from cationic collagen sponges mineralised for 1 day (Left bar: 500 nm. Right bar: 200 nm). Intrafibrillar mineralisation of cationic collagen with PAH-ACP was more rapid than

unmodified collagen; fairly extensive intrafibrillar mineralisation was evident after 1 day. **e**) TEM of leaflets from cationic collagen sponges mineralised by PAH-ACP for 7 days (Left bar: 500 nm. Right bar: 200 nm). Heavily mineralised cross-banded collagen could be identified.

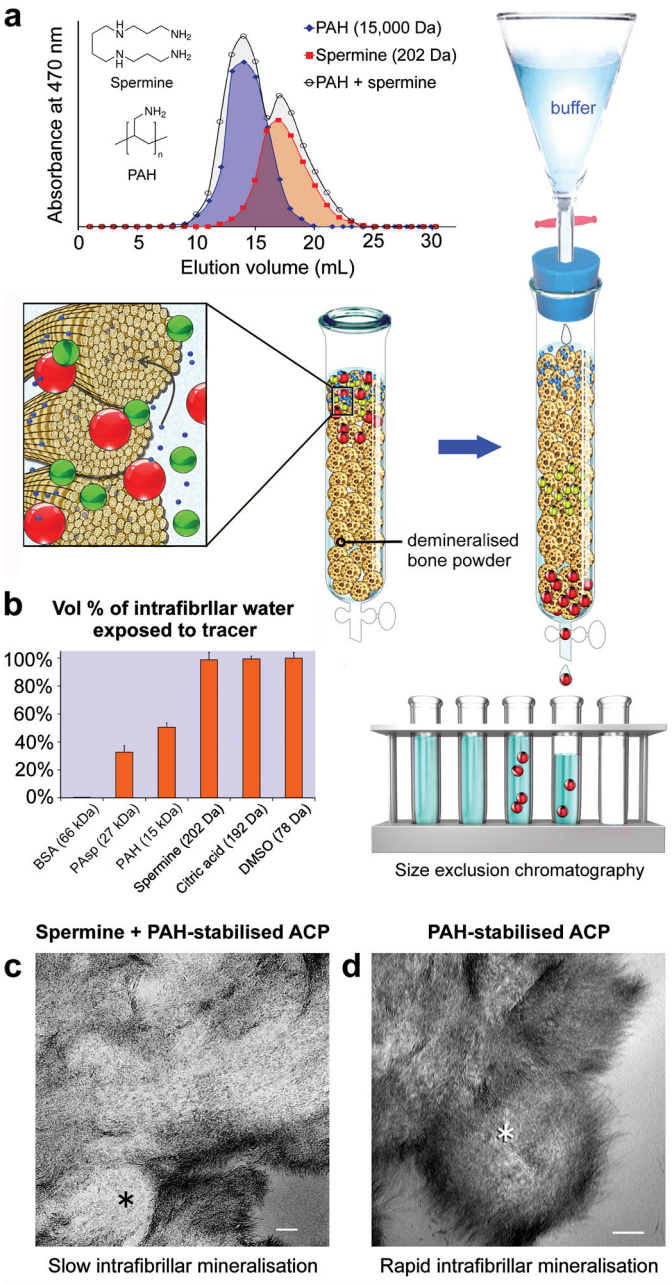

Figure 4.

The effects of inclusion of a short-chain polyamine (spermine) on collagen mineralisation with PAH-ACP. **a**) Size exclusion chromatography showing elution profiles of PAH (long-chain polyamine), spermine, and PAH/spermine mixture. Background illustrates the procedures involved. **b**) Percentage of collagen intrafibrillar volume penetrable by BSA (high molecular weight control), PAsp, PAH, spermine, citric acid, and DMSO (low molecular weight control) at pH 7.4. **c**) TEM of a leaflet from unstained collagen sponge mineralised for 7 days with PAH-ACP, with 0.3 mg/mL spermine added to the mineralisation medium (bar: 100 nm). Intrafibrillar mineralisation was delayed and sparse,

as seen in the cross section of a collagen fibril (asterisk). **d**) TEM of a leaflet from unstained collagen sponge mineralised for 7 days with PAH-ACP without spermine (bar: 100 nm). Cross section of a fibril (asterisk) shows profuse intrafibrillar mineralisation.

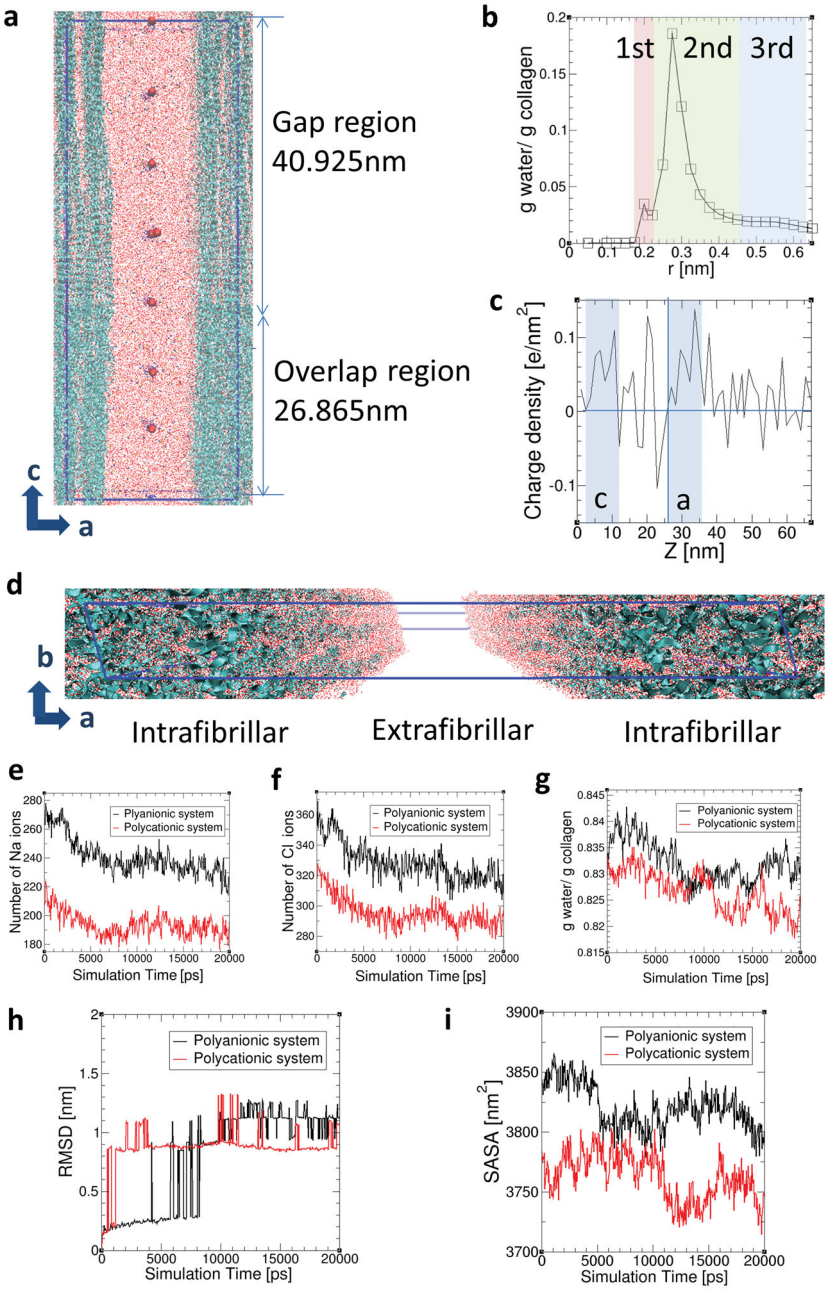

Figure 5.

Molecular dynamics simulations. **a**) Side view of simulated collagen fibrils with intrafibrillar and extrafibrillar spaces in polycationic solution. Blue ribbons and large red dots represent the collagen triple helices and bulky polycations, respectively. Small red dots, yellow dots and blue dots are water molecules, Na ions and Cl ions, respectively. The simulation box is indicated as the blue line. **b**) Intrafibrillar hydration layers surrounding collagen structures within the intrafibrillar regions. Distance r is the minimum distance between the water molecules and the collagen atoms. The 1st, 2nd and 3rd hydration layers were specified as (0–0.21 nm), (0.21–0.425 nm) and (0.425–0.625 nm) from the surface of

the collagen triple helices based on curvature and inflection points. The collagen structure together with these three hydration regions surrounding each collagen helix are considered as intrafibrillar regions. **c**) Charge density along the c axis of the collagen structures. **d**) Collagen structures with water molecules in the intrafibrillar regions and extrafibrillar region. Variations in the distribution of **e**) Na ions, **f**) Cl ions and **g**) water molecules in the intrafibrillar region ($r < 0.625$ nm) are shown as a function of simulation time in the polyanionic (black) and polycationic (red) systems, each of which has negatively- and positively-charged bulk particles in the extrafibrillar region. Variations in **h**) RMSD of collagen molecules and **i**) SASA of collagen structures over simulation time in the polyanionic (black) and polycationic (red) systems.

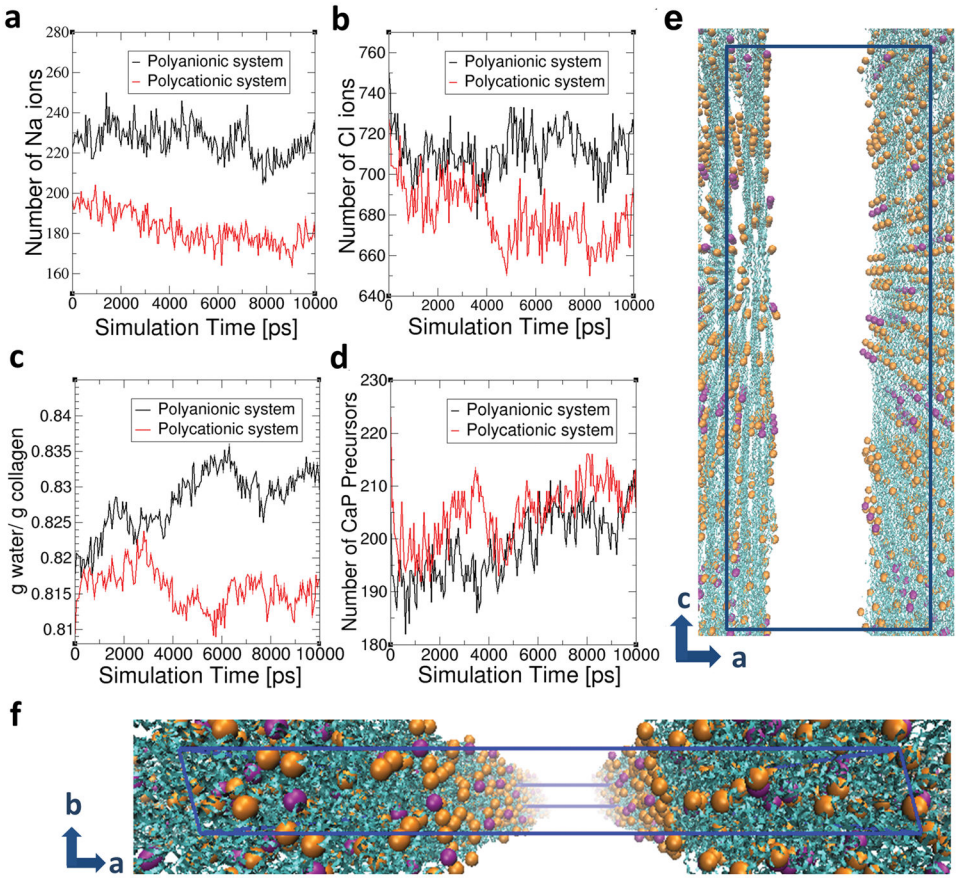

Figure 6.

Molecular dynamics simulations of the movement of ions, water molecules and mineralisation precursors that are simplified as Ca ions across the contracted collagen structures in the presence polyanionic and polycationic electrolytes, following the introduction of Ca ions into the system. The number of **a**) Na ions, **b**) Cl ions, **c**) water molecules and **d**) CaP precursors in the intrafibrillar region (r < 0.625 nm) are shown as a function of simulation time. **e**) and **f**) represent the collagen structures with intrafibrillar mineralisation precursors (simplified as Ca ions) in the polycationic system. Blue ribbons represent collagen structures and orange and purple dots presents Ca ions present in the intrafibrillar regions. Orange-coloured dots represent Ca ions in the 0.21–0.425 nm region, and purple-coloured dots represent Ca ions in the 0.425–0.625 nm region from the collagen structures. Water, Na ions, Cl ions, polycationic agents and Ca ions in the extrafibrillar regions are not shown in the figures for clearer viewing. Blue lined box indicates the simulation box, the dimensions of which are a = 24.2 nm, b = 2.83 nm, c = 67.79 nm with α = 90°, β = 90° and γ = 105.58°.